



Progress on phase equilibria of the Al–Si–Zr system at 700 and 900 °C



Ya Liu ^{a, b}, Maoyou Tang ^a, Changjun Wu ^a, Jianhua Wang ^{a, b}, Xuping Su ^{a, b, *}

^a Key Laboratory of Materials Surface Science and Technology of Jiangsu Province, Changzhou University, Changzhou 213164, China

^b Jiangsu Collaborative Innovation Center of Photovoltaic Science and Engineering, Changzhou University, Changzhou 213164, China

ARTICLE INFO

Article history:

Received 25 May 2016

Received in revised form

12 September 2016

Accepted 13 September 2016

Available online 14 September 2016

Keywords:

Ternary alloy system

Phase equilibria

Intermetallics

Microstructure

ABSTRACT

Phase equilibria of the Al–Si–Zr system were investigated using equilibrated alloys. All alloys were studied by X-ray powder diffraction, scanning electron microscopy and energy dispersive spectroscopy. The ternary phase τ_1 was found at 700 and 900 °C, while the τ_2 phase was only identified at 900 °C. 12 three-phase regions were experimentally determined in isothermal sections of the Al–Si–Zr system at both 700 and 900 °C. The solubility of Si in the intermediate and solution phases (i.e. Al_3Zr , Al_2Zr , Al_3Zr_2 , AlZr_3 , $\alpha\text{-Al}$ and (Zr)) at the Al–Zr side is limited, whereas the solubility of Al in the Si–Zr intermetallic (except the Si_2Zr_3 phase) is reverse. In addition, Al in the αSiZr phase at 900 °C decreased to 0.5 at.% from 10.3 at.% at 700 °C.

© 2016 Elsevier B.V. All rights reserved.

1. Introduction

Al–Si alloys are well known casting alloys and widely used as structural materials for all ranges of automotive applications, such as engine blocks, cylinder heads, chassis, driveline or heat shields [1–3]. To improve their high temperature performance small additions of zirconium are often added to Al based alloy due to the precipitation of ordered ZrAl_3 particles during aging procedure [4–10]. On the other hand, a purification process using an Al–Si solvent combined with electromagnetic solidification showed outstanding results in terms of purifying Si more economically and efficiently [11,12]. Small amounts of Zr were used as additives to strength B removal in the Al–Si solvent purification procedure [13,14]. The precipitation behaviors of phases in Al–Si–Zr alloy have received wide attention [4,8,9,15]. To understand the microstructure and subsequent property enhancement of Al-base alloys, knowledge on phase equilibrium of the ternary Al–Si–Zr system and a reliable Al–Si–Zr related multicomponent thermodynamic database is necessary. Concerning the ternary Al–Si–Zr system, experimental information is restricted to the partial isothermal section diagram from 700 °C to 1200 °C [16–18], and is limited to the Al-rich part. Takayuki Hirano et al. [19] have calculated the ternary system using first-principles method, but their results

remain disagreement with the rare experiment data. Therefore, it is necessary to investigate the ternary system by experiment.

In the present work, isothermal sections of the Al–Si–Zr system in the entire composition range at 700 °C and 900 °C have been established experimentally with techniques combining optical microscopy, scanning electron microscopy with energy dispersive X-ray spectroscopic capability (SEM-EDS), and X-ray diffraction. This work is essential to accumulate the required phase equilibria data for construction the Al–Si–Zr related thermodynamic database.

2. Literature data

2.1. Al–Si–Zr related binary systems

The three constituting binaries in the Al–Si–Zr ternary system, Al–Si, Al–Zr and Si–Zr systems are shown in Fig. 1. The Al–Si system was optimized by Dörner et al. [20], Chakraborti and Lukas [21] and Gröbner et al. [22]. The one accepted in this work was from Gröbner et al. [22], who optimized the Al–Si system on the basis of the latest thermodynamic function of pure elements compiled by Dinsdale [23], as shown in Fig. 1(a). No binary compound was included in this system. The equilibrium phase diagram of the Al–Zr system has been reviewed by Saunders and Rivlin [24], Murray et al. [25], Okamoto [26] and Wang et al. [27]. Fischer and Colinet [28] have recently updated thermodynamic modeling of the Al–Zr system using the CALPHAD approach, which has been shown in Fig. 1(b). Ten intermetallic compounds, i.e. Al_2Zr , Al_3Zr , AlZr ,

* Corresponding author. Key Laboratory of Materials Surface Science and Technology of Jiangsu Province, Changzhou University, Changzhou 213164, China.

E-mail address: jspxing@cczu.edu.cn (X. Su).

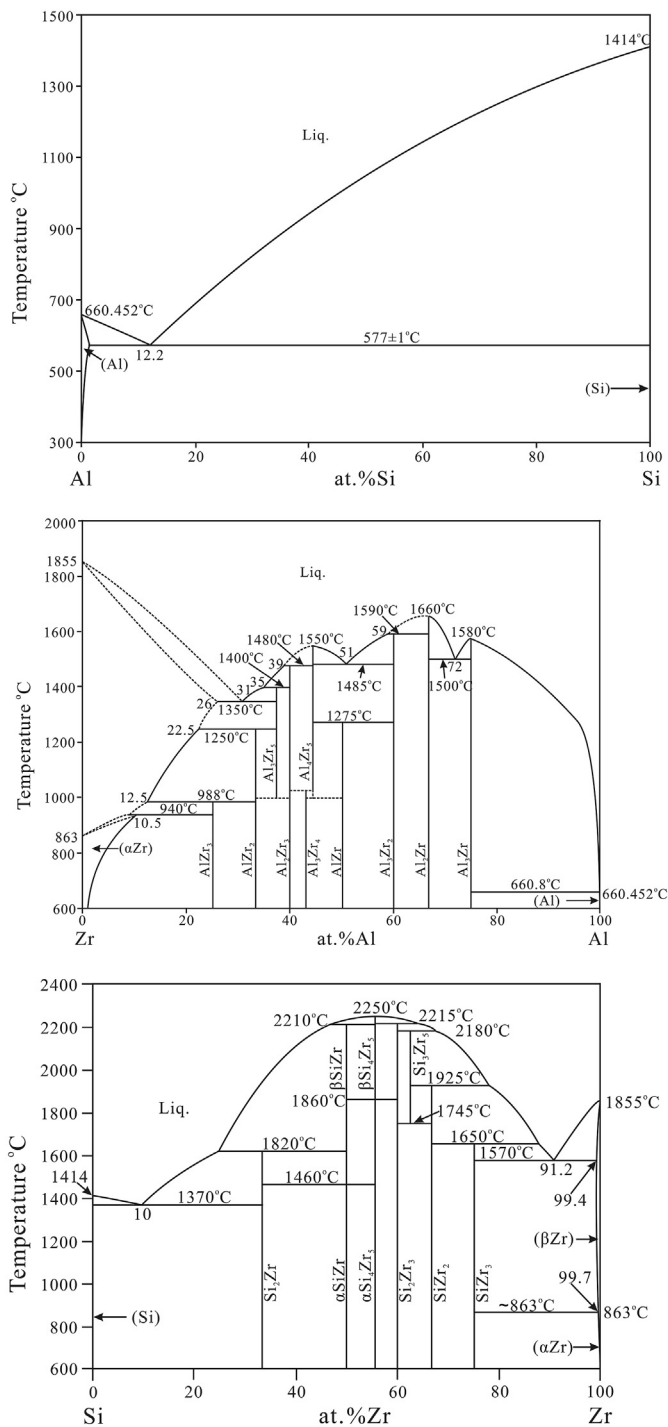


Fig. 1. Binary phase diagrams constituting the Al–Si–Zr ternary system. (a) Al–Si system [22], (b) Al–Zr system [28], (c) Si–Zr system [29].

Al_3Zr_2 , Al_4Zr_5 , Al_3Zr_4 , Al_3Zr_5 , Al_2Zr_3 , AlZr_2 and AlZr_3 , are reported in the system. Their homogeneity ranges are quite restricted. Except Al_4Zr_5 and Al_3Zr_5 , all the other phases are stable at both 700 and 900 °C.

The Si–Zr binary system [29] shown in Fig. 1(c) has seven intermetallic compounds, i.e. Si_4Zr_5 , SiZr , Si_2Zr_3 , Si_2Zr , Si_3Zr_5 , SiZr_2 and SiZr_3 . These intermetallics are stable at both 700 and 900 °C except the Si_3Zr_5 phase. SiZr and Si_4Zr_5 compounds undergo transformations $\alpha\text{SiZr} \rightarrow \beta\text{SiZr}$ and $\alpha\text{Si}_4\text{Zr}_5 \rightarrow \beta\text{Si}_4\text{Zr}_5$ respectively.

More information about the crystal structure of the binary phases is shown in Table 1.

2.2. The Al–Si–Zr ternary system

The isothermal section at 400, 500 and 525 °C of the Al–Si–Zr ternary phase diagram were reported by Drits et al. [32], however, the knowledge is limited to the Al-rich part containing up to 1.73 at.% Si and 0.17 at.% Zr. The equilibrium phases in Al–Si–Zr ternary alloys containing up to 60 at.% Zr were determined at 700 °C by Raman and Schubert [17]. Schob and Nowotny [16] studied the isothermal sections of the Al–Si–Zr system between 550 and 1200 °C, the sole complete isothermal section was replicated in Fig. 2. By analyzing microstructure and composition of binary and ternary intermetallic compound formed in ternary diffusion couples of Zr and Al–Si eutectic alloy, the Zr-rich corner of the isothermal sections was constructed tentatively by Jain and Gupta [18]. Later on, Hirano et al. [19] determined the phase equilibria of the Al–Si–Zr ternary system based on the CALPHAD method. The phase diagram contains three ternary compounds, denoted as τ_1 , τ_2 and τ_3 . The τ_1 phase, with its composition in the range 7.5–10 at.% Si and 25 at.% Zr, appears in all of the experimental temperatures. The second ternary phase τ_2 occurring at 10–12.5 at.% Al and 50 at.% Zr has been reported by Schob et al. [16] at 1200 °C. The τ_2 phase was observed in the interface of Zr/Al–Si diffusion annealed at 900 °C and above, while it disappeared when the annealing temperature was 700 °C and 800 °C. Meanwhile, this phase was not reported in the isothermal section at 700 °C [17]. According to XRD analysis, τ_2 is the binary high-temperature modification of ZrSi (CrB-type), which is stabilized at lower temperatures by substitution of Al for Si [16]. A ternary phase τ_3 with the composition $\text{Al}_4\text{Zr}_3\text{Si}_5$ was included in the isothermal section at 700 and 900 °C reported by Raman and Schubert [17]. The τ_3 phase was proposed to form by a ternary peritectic reaction, $L + \text{ZrSi} + \tau_1 \leftrightarrow \tau_3$. This phase was reported to be unstable above 900 °C in the diffusion couple analyzing, and was proposed to be unstable above 950 °C by Harmelin et al. [33] in their assessment of the ternary phase diagram of the Al–Si–Zr system. Another two phases, denoted as $\text{Zr}_2\text{Al}_{0.5}\text{Si}_{0.5}$ and $\text{ZrAl}_{0.5}\text{Si}_{0.5}$, was reported by XRD analyzing of annealed alloys. In particular, $\text{Zr}_2\text{Al}_{0.5}\text{Si}_{0.5}$ is not a ternary phase, but solid solutions $(\text{Al},\text{Si})\text{Zr}_2$ extending from binary SiZr_2 . The $\text{ZrAl}_{0.5}\text{Si}_{0.5}$ phase has the same structure with τ_2 , which exists at 1200 °C [16] as well as 700 °C [7]. The phases have different designations in different references, more detailed information on crystallographic data of phases in the Al–Si–Zr system has been listed in Table 2.

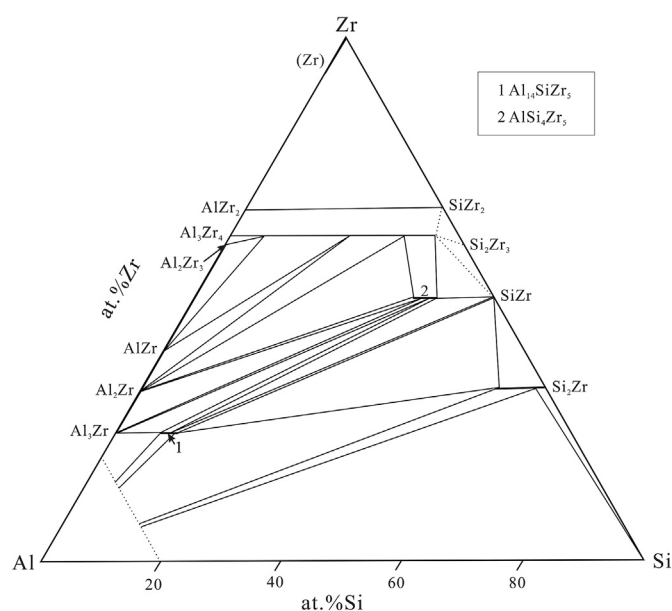
3. Experimental procedure

More than 70 alloy samples were prepared to study the 700 and 900 °C isothermal sections of the Al–Si–Zr ternary system. Purity of the raw materials, i.e. Zr columns, and Al and Si particles, was 99.99 wt%. The mixture of raw materials (10 g in total for each sample), with the weight of each constituent precisely measures, was melted under argon atmosphere using a non-consumable tungsten electrode. The ingots were repeated three times to improve their homogeneity. Buttons with weight loss under 1% after melting were conducted with the following thermal treatment. Plate specimen cut from the button ingots was put into corundum crucible and then sealed in an evacuated quartz tube under an argon gas atmosphere. The quartz tube samples were placed in the annealing furnace and kept at 700 and 900 °C for 30 days, respectively, followed by quenching in water to preserve the equilibrium state at the annealing temperature.

All the annealed samples were divided into two parts, one part

Table 1
Crystallographic data of binary phases in the Al–Si–Zr system.

System	Phase	Structure type	Space group	Lattice parameters(nm)			Refs.	
				a	b	c		
Al–Zr	Al ₃ Zr	AuCu ₃	Pmm	0.39993	0.39993	1.7283	[30]	
	Al ₂ Zr	MgZn ₂	P6 ₃ /mmc	0.52824	0.52824	0.87482	[30]	
	Al ₃ Zr ₂	Al ₃ Zr ₂	Fdd2	0.9601	1.3906	0.5574	[30]	
	AlZr	CrB	Cmcm	0.3359	1.0887	0.4274	[30]	
	Al ₂ Zr ₃	Al ₂ Zr ₃	P4 ₂ /mnm	0.7630	0.7630	0.6998	[30]	
	Al ₃ Zr ₄	Al ₃ Zr ₄	P6/mmm	0.5433	0.5433	0.5390	[30]	
	AlZr ₂	Ni ₂ In	P6 ₃ /mmc	0.48939	0.48939	0.59283	[30]	
	AlZr ₃	AuCu ₃	Pmm	0.4372	0.4372	0.4372	[30]	
	Si–Zr	Si ₂ Zr	Al ₂ Cu	I4/mcm	0.6609	0.6609	0.5298	[31]
		αSiZr	FeB	Pnma	0.6995(3)	0.3786(2)	0.5296(3)	[31]
αSi ₄ Zr ₅		Si ₄ Zr ₅	P4 ₁ 2 ₁ 2	0.7123(1)	0.7123(1)	1.3002(1)	[31]	
Si ₂ Zr ₃		U ₃ Si ₂	P4/mbm	0.7082	0.7082	0.3714	[31]	
SiZr ₂		CuAl ₂	I4/mcm	0.6609(3)	0.6609(3)	0.5298(3)	[31]	
SiZr ₃		Ti ₃ P	P4 ₂ /n	1.101	1.101	0.545	[31]	

**Fig. 2.** Phase relations in the ternary Al–Si–Zr system at 700 °C [16].

of samples were prepared by traditional way for microstructure examination and the other part of samples were prepared for X-ray

diffraction. The microstructure and phases' composition analysis were performed in a JSM–6510 scanning electron microscopy (SEM) equipped with OXFORD energy dispersive X-ray spectrometer (EDS), with probe diameter of 1 μm and an accelerating voltage of 20 kV. The compositions reported herein were averages of at least five measurements. At the same time, the constituent phases in the alloys were carefully studied by analyzing X-ray diffraction (XRD) patterns generated by a D/max 2500 PC X-ray diffractometer with Cu K_α radiation and a step increase of 0.02° in the 2θ angle. Si powders were used as external calibrated standard. Jade software package was used to index and calculate the X-ray diffraction (XRD) patterns.

4. Result and discussion

4.1. Phase equilibria of the Al–Si–Zr system at 700 °C

The microstructures and XRD patterns of typical Al–Si–Zr alloys annealed at 700 °C for 30 days are presented in Fig. 3(a–l) and Figs. 4–7, respectively. Table 3 summarizes the nominal compositions of the alloys and the phases in equilibrium which were identified by a combination of XRD and SEM-EDS.

In the Al₃₀Si₅₄Zr₁₆ (at.%) alloy, three phases (α-Al + Si + Si₂Zr) exhibited in Fig. 3(a) were identified based on their brightness on grayscale images and chemical composition. Fig. 3(b) shows the three-phase microstructure (α-Al + τ₁ + Si₂Zr) of the Al₄₀Si₃₇Zr₂₃ (at.%) alloy. The τ₁ phase had also been evidenced in the other

Table 2
Crystallographic data of phases in the Al–Si–Zr system.

Phase	Other designation	Structure type	Space group	Temperature (°C)	Method	Refs.
τ ₁	(Zr(Al _{1-x} Si _x) ₃ , 0.1 ≤ x ≤ 0.4) Zr ₂ Al ₅ Si	TiAl ₃	I4/mmm	700,1200	Annealed alloy, XRD	[16,17,19]
				700,800,900, 1000,1100	Diffusion couple, EPMA	[18]
				1200	Annealed alloy, XRD	[16] ^a
τ ₂	(Zr(Al _x Si _{1-x}), 0.2 ≤ x ≤ 0.25)	CrB	Cmcm	900,1000,1100	Diffusion couple, EPMA	[18]
τ ₃	Zr ₃ Al ₄ Si ₅	(Zr _{0.75} Al _{0.25}) (Al _{0.38} Si _{0.62}) ₂	I4 ₁ /amd	700	Annealed alloy, XRD	[17]
				900	Diffusion couple, EPMA	[18]
Zr ₂ Al _{0.5} Si _{0.5} ZrAl _{0.5} Si _{0.5} ^c	CuAl ₂ TII	I4/mcm Cmcm		≤950	Thermodynamic assessment	[33]
					Annealed alloy, XRD	[16] ^b
					Annealed alloy, XRD	[16,17]

^a According to the XRD analysis, τ₂ is the binary high-temperature modification of ZrSi (CrB-type), which is stabilized to lower temperatures by substitution of Al for Si.

^b Not a ternary phase, but solid solutions (Al,Si)Zr₂ extending from binary SiZr₂.

^c This phase has the same structure with τ₂. ZrAl_{0.5}Si_{0.5} exists at 1200 °C [16] as well as 700 °C [7].

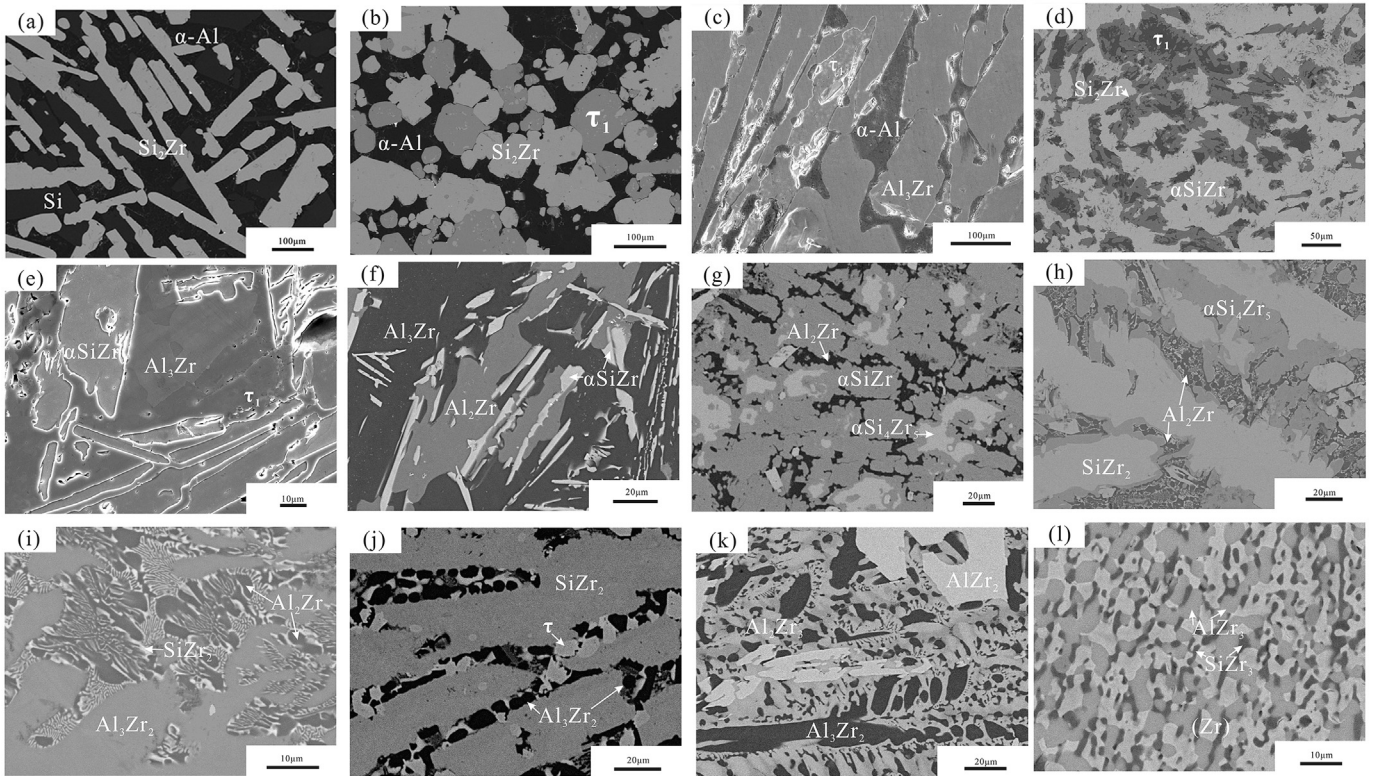


Fig. 3. Microstructure images of alloys annealed at 700 °C, in back scattered electrons (BSE), (a) the $\text{Al}_{30}\text{Si}_{54}\text{Zr}_{16}$ (at.%) alloy, (b) the $\text{Al}_{40}\text{Si}_{37}\text{Zr}_{23}$ (at.%) alloy, (d) the $\text{Al}_{18}\text{Si}_{44}\text{Zr}_{38}$ (at.%) alloy, (f) the $\text{Al}_{66}\text{Si}_{5}\text{Zr}_{29}$ (at.%) alloy, (g) the $\text{Al}_{24}\text{Si}_{29}\text{Zr}_{47}$ (at.%) alloy, (h) the $\text{Al}_{24}\text{Si}_{25}\text{Zr}_{51}$ (at.%) alloy, (i) the $\text{Al}_{56}\text{Si}_{14}\text{Zr}_{40}$ (at.%) alloy, (j) the $\text{Al}_{24}\text{Si}_{19}\text{Zr}_{57}$ (at.%) alloy, (k) the $\text{Al}_{38}\text{Si}_{5}\text{Zr}_{57}$ (at.%) alloy, (l) the $\text{Al}_{15}\text{Si}_{5}\text{Zr}_{80}$ (at.%) alloy; in secondary electrons (SEI), (c) the $\text{Al}_{74}\text{Si}_{6}\text{Zr}_{20}$ (at.%) alloy, (e) the $\text{Al}_{50}\text{Si}_{17}\text{Zr}_{33}$ (at.%) alloy.

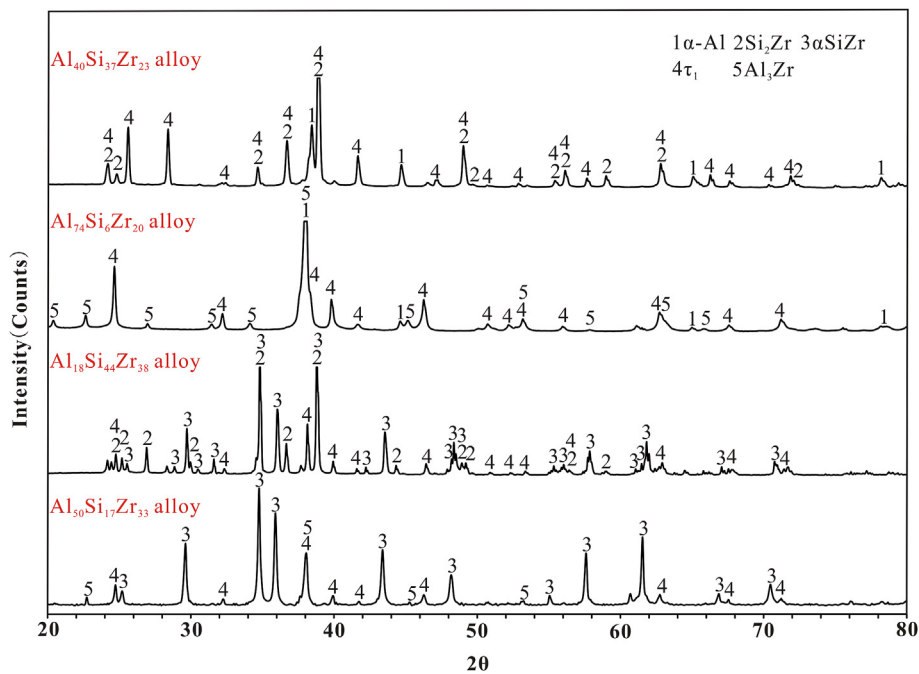


Fig. 4. XRD patterns of the alloys (○) the $\text{Al}_{40}\text{Si}_{37}\text{Zr}_{23}$ (at.%) alloy, (○) the $\text{Al}_{74}\text{Si}_{6}\text{Zr}_{20}$ (at.%) alloy, (○) the $\text{Al}_{18}\text{Si}_{44}\text{Zr}_{38}$ (at.%) alloy and (○) the $\text{Al}_{50}\text{Si}_{17}\text{Zr}_{33}$ (at.%) alloy which were annealed at 700 °C for 30 days.

three-phase equilibria of ($\alpha\text{-Al} + \tau_1 + \text{Al}_3\text{Zr}$), ($\text{Si}_2\text{Zr} + \tau_1 + \alpha\text{SiZr}$) and ($\text{Al}_3\text{Zr} + \tau_1 + \alpha\text{SiZr}$) found in the $\text{Al}_{74}\text{Si}_{6}\text{Zr}_{20}$, $\text{Al}_{18}\text{Si}_{44}\text{Zr}_{38}$ and $\text{Al}_{50}\text{Si}_{17}\text{Zr}_{33}$ alloys respectively (Fig. 3(c–e)). The ternary phase τ_1 ,

with TiAl_3 structural type, was first reported by Raman and Schubert. XRD patterns visualized in Fig. 4 confirmed the existence of this ternary phase. As shown in Fig. 3(f), the three-phase

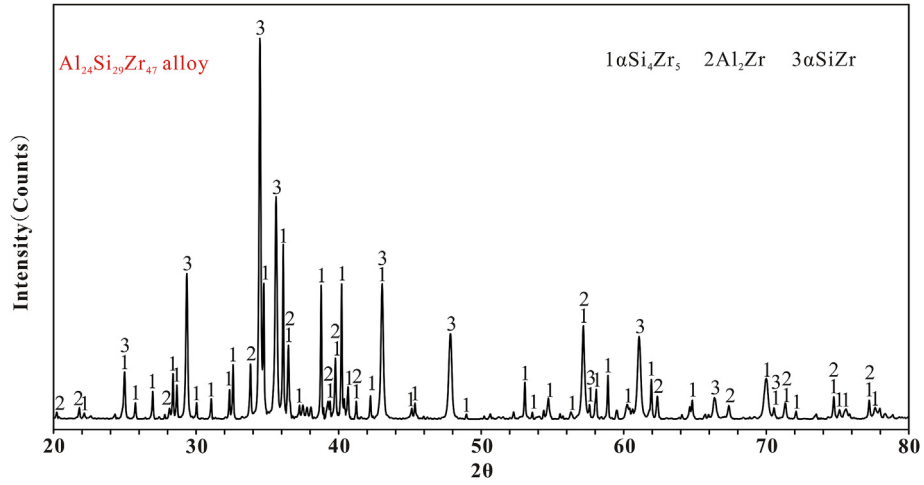


Fig. 5. XRD patterns of the $\text{Al}_{24}\text{Si}_{29}\text{Zr}_{47}$ (at.%) alloy.

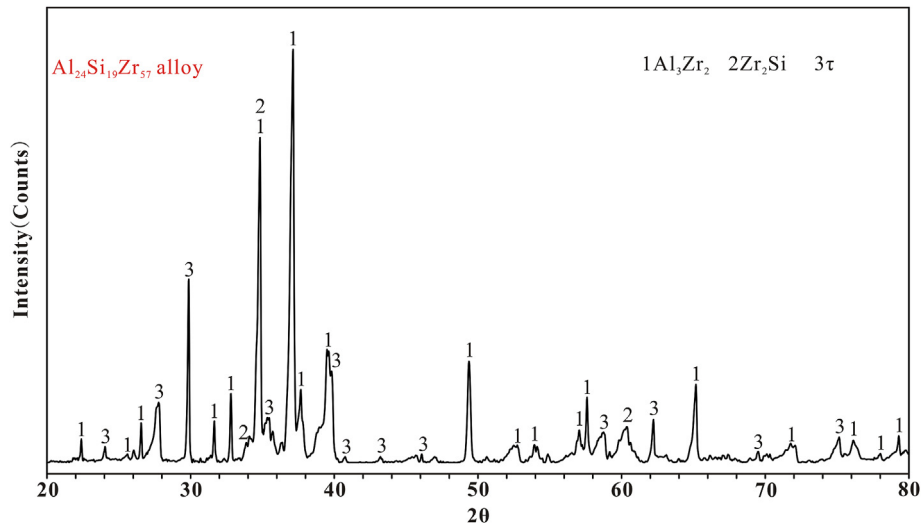


Fig. 6. XRD patterns of the $\text{Al}_{24}\text{Si}_{19}\text{Zr}_{57}$ (at.%) alloy.

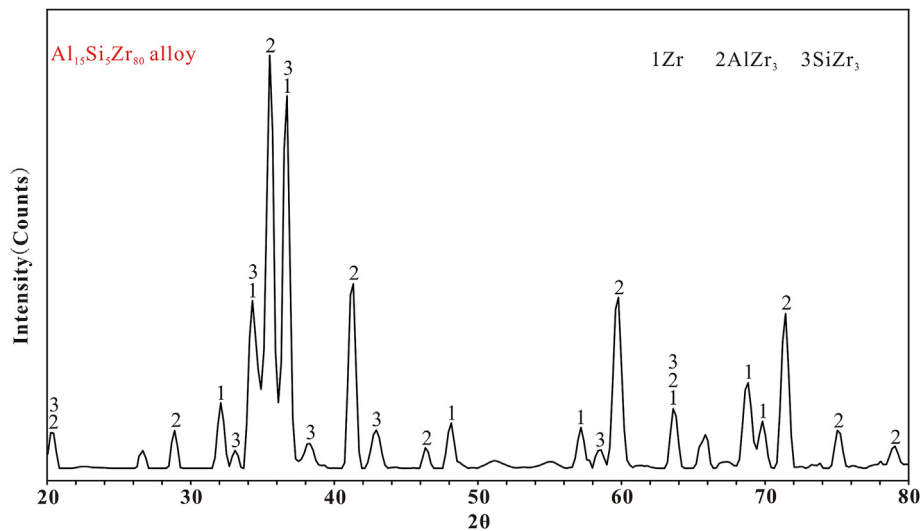


Fig. 7. XRD patterns of the $\text{Al}_{15}\text{Si}_5\text{Zr}_{80}$ (at.%) alloy.

Table 3
Equilibrium compositions of the Al–Si–Zr ternary system determined in the present work.

T (°C)	Designed composition (at.%)	Phase identified phase 1/Phase 2/Phase 3	Composition (at.%)						
			Phase 1		Phase 2		Phase 3		
			Si	Zr	Si	Zr	Si	Zr	
700	Al ₃₀ Si ₅₄ Zr ₁₆	α -Al/Si/Si ₂ Zr	2.7	0.1	100.0	0	60.1	32.4	
	Al ₄₀ Si ₃₇ Zr ₂₃	α -Al/ τ_1 /Si ₂ Zr	2.4	0.1	12.8	26.7	56.9	32.1	
	Al ₇₄ Si ₆ Zr ₂₀	α -Al/ τ_1 /Al ₃ Zr	2.5	0.2	11.2	26.5	0.5	24.4	
	Al ₁₈ Si ₄₄ Zr ₃₈	Si ₂ Zr/ τ_1 / α SiZr	56.4	32.4	12.3	27.4	46.1	49.7	
	Al ₅₀ Si ₁₇ Zr ₃₃	Al ₃ Zr/ τ_1 / α SiZr	0.5	24.8	11.0	27.2	43.6	49.9	
	Al ₆₆ Si ₅ Zr ₂₉	Al ₃ Zr/Al ₂ Zr/ α SiZr	0.4	25.2	0.4	32.8	40.8	49.5	
	Al ₂₄ Si ₂₉ Zr ₄₇	α Si ₄ Zr ₅ /Al ₂ Zr/ α SiZr	37.4	54.1	0.4	33.1	39.6	50.1	
	Al ₂₄ Si ₂₅ Zr ₅₁	α Si ₄ Zr ₅ /Al ₂ Zr/SiZr ₂	32.7	53.9	0.3	33.3	32.2	64.5	
	Al ₅₆ Si ₄ Zr ₄₀	Al ₃ Zr ₂ /Al ₂ Zr/SiZr ₂	0.5	39.6	0.3	33.4	31.3	64.6	
	Al ₂₄ Si ₁₉ Zr ₅₇	Al ₃ Zr ₂ / τ /SiZr ₂	0.4	39.9	20.8	64.7	31.2	64.8	
	Al ₃₈ Si ₅ Zr ₅₇	Al ₃ Zr ₂ /AlZr ₂ /Al ₂ Zr ₃	0.3	40.1	13.5	65.2	2.6	59.6	
	Al ₁₅ Si ₅ Zr ₈₀	AlZr ₃ /SiZr ₃ /(Zr)	0	75.5	15.1	75.1	0	97.2	
	900	Al ₃₀ Si ₅₄ Zr ₁₆	α -Al/Si/Si ₂ Zr	24.8	0.3	100.0	0	62.3	33.1
		Al ₄₀ Si ₃₇ Zr ₂₃	α -Al/ α SiZr/Si ₂ Zr	21.4	0.3	50.1	49.6	57.3	32.8
Al ₇₄ Si ₆ Zr ₂₀		α -Al/ τ_1 /Al ₃ Zr	2.9	0.6	10.5	26.6	0.5	24.9	
Al ₄₁ Si ₂₉ Zr ₃₀		α -Al/ τ_1 / α SiZr	19.4	0.5	11.8	26.1	49.9	49.7	
Al ₄₀ Si ₂₄ Zr ₃₆		Al ₃ Zr/ τ_1 / α SiZr	0.6	25.0	11.5	27.7	49.8	49.8	
Al ₆₆ Si ₅ Zr ₂₉		Al ₃ Zr/Al ₂ Zr/ τ_2	0.5	25.4	0.3	32.9	38.8	49.9	
Al ₅ Si ₄₃ Zr ₅₂		α Si ₄ Zr ₅ / τ_2 / α SiZr	43.4	55.4	39.4	50.1	49.3	50.2	
Al ₂₄ Si ₂₆ Zr ₅₀		α Si ₄ Zr ₅ /Al ₂ Zr/SiZr ₂	33.1	53.5	0.3	33.1	31.5	64.4	
Al ₅₆ Si ₄ Zr ₄₀		Al ₃ Zr ₂ /Al ₂ Zr/SiZr ₂	0.5	39.5	0.3	33.1	28.2	64.3	
Al ₁ Si ₃₉ Zr ₆₀		α Si ₄ Zr ₅ /Si ₂ Zr ₃ /SiZr ₂	42.1	55.3	40.0	59.5	33.1	65.7	
Al ₃₈ Si ₅ Zr ₅₇		Al ₃ Zr ₂ /AlZr ₂ /Al ₂ Zr ₃	0.4	40.2	12.2	66.0	1.9	60.2	
Al ₁₅ Si ₅ Zr ₈₀		AlZr ₃ /SiZr ₃ /(Zr)	0	75.9	16.2	76.1	0.1	94.3	

equilibrium of (Al₃Zr + Al₂Zr + α SiZr) was observed in the Al₆₆Si₅Zr₂₉ alloy. The Al₂₄Si₂₉Zr₄₇, Al₂₄Si₂₅Zr₅₁ and Al₅₆Si₄Zr₄₀ alloys located in the three-phase equilibria of (Al₂Zr + α Si₄Zr₅ + α SiZr), (α Si₄Zr₅ + Al₂Zr + SiZr₂) and (Al₃Zr₂ + Al₂Zr + SiZr₂) respectively (Fig. 3(g–i)). XRD pattern of the Al₂₄Si₂₉Zr₄₇ alloy was presented in Fig. 5, three-phase equilibria between Al₂Zr + α Si₄Zr₅ + α SiZr was confirmed. In the Al₂₄Si₁₉Zr₅₇ alloy, three phases (Al₃Zr₂ + τ + SiZr₂) were observed in Fig. 3(j) and the XRD patterns

are shown in Fig. 6. Seen from Fig. 6, characteristic peaks of the Al₃Zr₂ and SiZr₂ phases are clearly evidenced, however, the other peaks cannot be indexed with the SiZr₃ phase. As its structure is not clear at this stage, it has been denoted as “ τ ” in this study. Meanwhile, two three-phase equilibria of (Al₃Zr₂ + AlZr₂ + Al₂Zr₃) and (AlZr₃ + SiZr₃ + (Zr)) were found in the Al₃₈Si₅Zr₅₇ and Al₁₅Si₅Zr₈₀ alloys respectively (Fig. 3(k) and (l)) and the XRD patterns of Al₁₅Si₅Zr₈₀ are shown in Fig. 7.

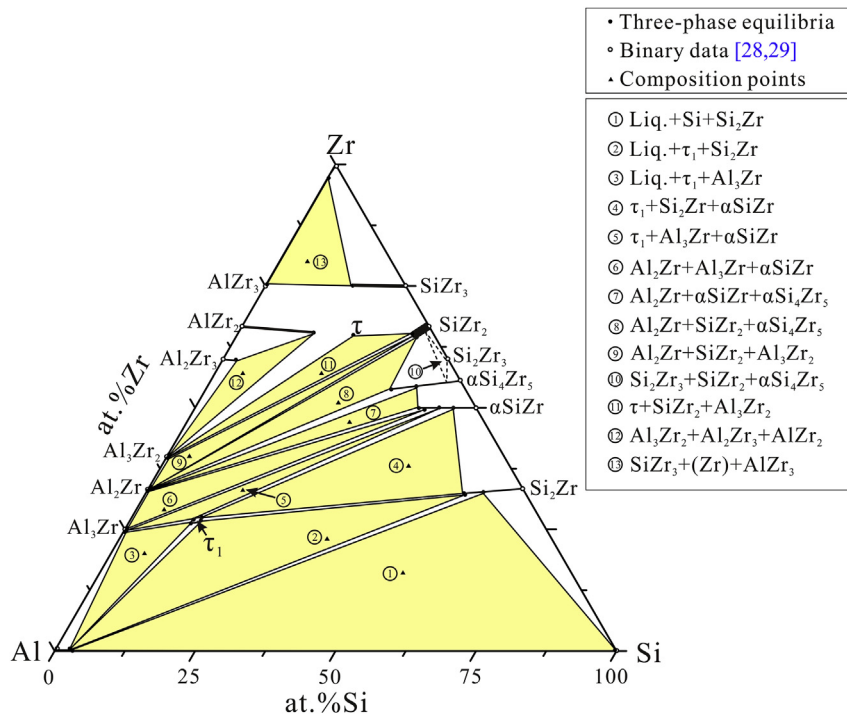


Fig. 8. Phase relations in the ternary Al–Si–Zr system, constructed from samples annealed at 700 °C.

Based on the experimental information mentioned above, isothermal section of ternary Al–Si–Zr system at 700 °C was constructed in Fig. 8. Undetermined three-phase equilibria are shown in Fig. 8 in dashed lines. The solubility of Si in the intermediate and solution phases (i.e. Al₃Zr, Al₂Zr, Al₃Zr₂, α-Al and (Zr)) at the Al–Zr side is limited, whereas the solubility of Si in the Zr rich corner (especially for the AlZr₂ and AlZr₃ phases) and the solubility of Al in the Si–Zr intermetallic (except Si₂Zr₃ phase) is reverse. The solubility of Si in Al₂Zr₃, AlZr₂ and AlZr₃ phases was measured to be about 2.6 at.%, 13.5 at.% and 0.0 at.% respectively. The solubility of Al in SiZr₃, SiZr₂, αSi₄Zr₅, αSiZr and Si₂Zr was found to be about 9.8 at.%, 4.1 at.%, 13.4 at.%, 10.3 at.%, 11.2 at.%. The solubility range in the intermetallic compounds has been compared in Table 3. The present study gets close to the result of Raman and Shubert' investigation [17]. In addition, as indicated in Fig. 1(b), the AlZr and Al₃Zr₄ phases in the Al–Zr binary system forms as a result of eutectoid reactions, Al₃Zr₂+Al₄Zr₅ ↔ AlZr and Al₄Zr₅ +Al₂Zr₃ ↔ Al₃Zr₄ respectively. These reactions may be hindered due to the ternary addition of Si in the Al–Zr alloys, so the AlZr and Al₃Zr₄ phases were not identified in this study. In agreement with the work of ref. [18], only one ternary phase τ₁ was identified in the microstructures of Al–Si–Zr alloys annealed at 700 °C. The ternary phase τ₃, which was reported by Raman and Shubert, was not found in the present work. This is in agreement with Jain and

Gupta's study [18]. Compared with the isothermal section at 700 °C described in Ref. [17], the three-phase equilibria of (α-Al + Si + Si₂Zr), (α-Al + τ₁ + Al₃Zr), (Si₂Zr + τ₁ + αSiZr) and (Al₃Zr + Al₂Zr + αSiZr) were confirmed in the present work. As indicated in Fig. 8, the three-phase equilibrium of (α-Al + τ₁ + Si₂Zr), rather than the ternary compound τ₃ in Ref. [17], was reported in this work.

According to phase equilibrium between 550 and 1200 °C reported by Schob and Nowotny [16], continuous mutual solutions between SiZr₂ and AlZr₂ were constructed, and large solubility of Si in Al₃Zr₄ was evidenced. In this work, more than 20 alloys around the AlZr₃, AlZr₂ and SiZr₃ area have been prepared, however, these alloys are quite difficult to get equilibrium, so no more information can be provided in this region. According to XRD analysis by Schob and Nowotny [16], solid solutions AlSi₄Zr₅ is extended from binary αSiZr phase, so the equilibrium between αSiZr, Al₂Zr, Al₃Zr, Si₂Zr and τ₁ agrees well with the present work. Phases SiZr₃ and αSi₄Zr₅, which were not reported in Ref. [16], have been observed in this study.

4.2. Phase equilibria of the Al–Si–Zr system at 900 °C

Experimental data of the Al–Si–Zr alloys annealed at 900 °C, which were determined based on SEM–EDS and XRD analysis, are

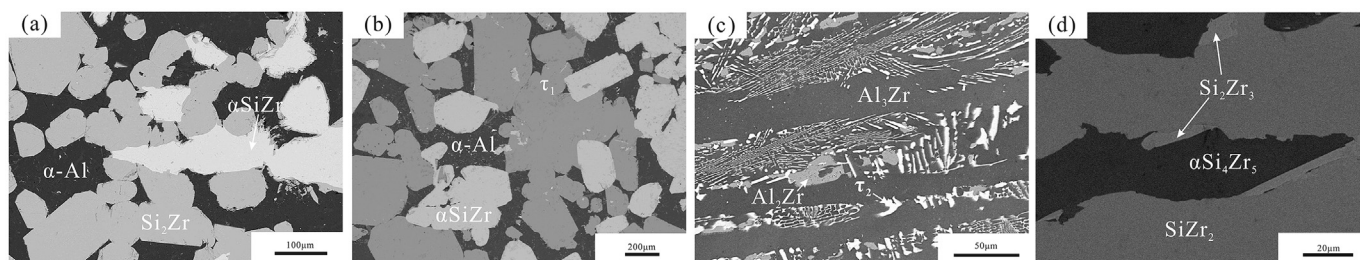


Fig. 9. Microstructure images of alloys annealed at 900 °C, in back scattered electrons (BSE), (a) the Al₄₀Si₃₇Zr₂₃ (at.%) alloy, (b) the Al₄₁Si₂₉Zr₃₀ (at.%) alloy, (c) the Al₆₆Si₅Zr₂₉ (at.%) alloy, (d) the Al₁Si₃₉Zr₄₀ (at.%) alloy.

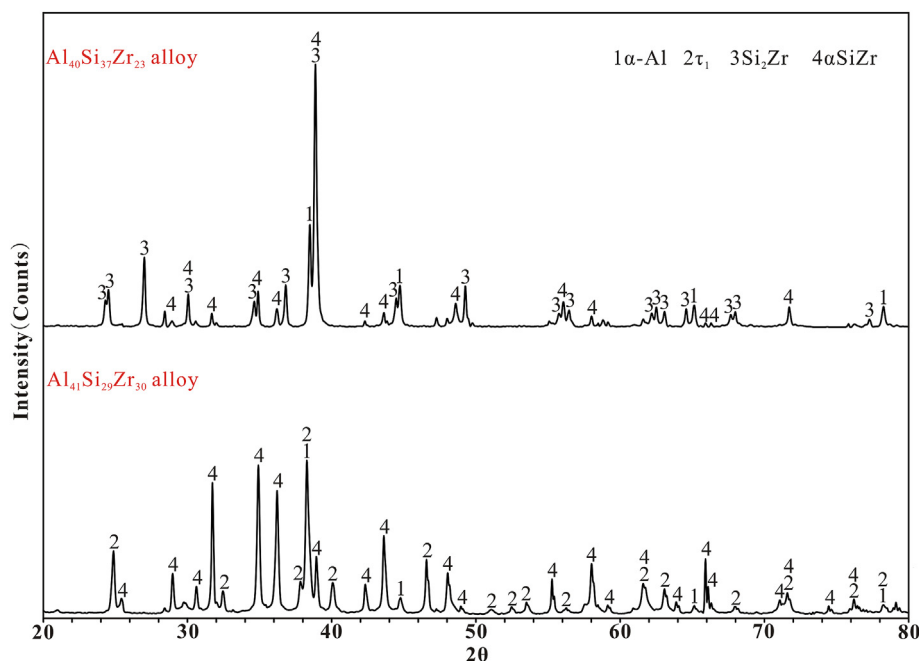


Fig. 10. XRD patterns of the alloys (⊙) the Al₄₀Si₃₇Zr₂₃ (at.%) alloy and (⊙) the Al₄₁Si₂₉Zr₃₀ (at.%) alloy which were annealed at 900 °C for 30 days.

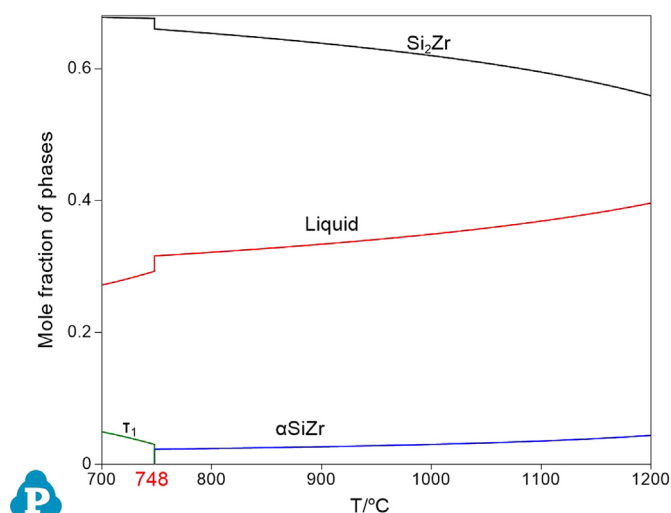


Fig. 13. Phase constituents of alloy $\text{Al}_{25}\text{Si}_{50}\text{Zr}_{25}$ from 700 to 1200 °C.

The phase equilibria of the Al–Si–Zr system at 900 °C are shown graphically in Fig. 12. The fields of the compound (τ_1 and τ_2) are identified. In similar to the phase relationship at 700 °C, the ternary compound τ_3 was not found, this is inconsistent with the results reported by Jain and Gupta [18]. As Fig. 12 indicated, the αSiZr phase equilibrated with the $\alpha\text{-Al}$ phase at 900 °C, which interrupted the equilibrium between the τ_1 phase and the Si_2Zr phase. In addition, due to the existence of the τ_2 , the three-phase equilibrium ($\text{Al}_2\text{Zr} + \alpha\text{Si}_4\text{Zr}_5 + \text{SiZr}$) was not identified. Coupling with the thermodynamic descriptions of the Al–Si [22], Al–Zr [28] and Si–Zr [29] binary systems, and Gibbs energy description of the τ_1 phase adopted from Ref. [19], phase equilibrium between τ_1 , liquid, SiZr and Si_2Zr phases was calculated with the Pandat software [34]. Phase constituents of alloy $\text{Al}_{25}\text{Si}_{50}\text{Zr}_{25}$ from 700 to 1200 °C are shown in Fig. 13. The change of tie line from τ_1 and Si_2Zr at 700 °C (ref. [17] and this work) to liquid and αSiZr at 900 °C (this work) has been modeled thermodynamically. As demonstrated in Fig. 13, this transformation would take place at 748 °C. However, the change of tie line from liquid and αSiZr at 900 °C back to τ_1 and Si_2Zr at 1200 °C (ref. [16]) was observed from the calculation. So it is necessary to add more experimental information on phase equilibrium at 1200 °C. However, it is beyond the scope of this work. Compared with the isothermal section of the Al–Si–Zr system at 700 °C, except the solubility of Al in the αSiZr phase at 900 °C decreased to 0.5 at.% from 10.3 at.% at 700 °C, no obvious change was found for the solubility ranges of the other compounds at these two temperatures.

5. Conclusions

The 700 °C and 900 °C isothermal sections of the Al–Si–Zr ternary system have been experimentally determined by using SEM-EDS and XRD techniques, and the main conclusions are

obtained as follows:

- 1) 12 three-phase regions were experimentally determined in isothermal sections of this system at both 700 and 900 °C.
- 2) The τ_1 phase (TiAl₃-type) was confirmed at both 700 and 900 °C, which the τ_2 phase (cubic CrB-type) was only identified at 900 °C.
- 3) The solubility of Si in the Al–Zr binary compounds (except Al_2Zr_3 and AlZr_2) and the solubility of Al in Si_2Zr_3 is extremely small. Al in the αSiZr phase at 900 °C decreased to 0.5 at.% from 10.3 at.% at 700 °C.

Acknowledgments

Financial supports from the National Science Foundation of China (Grant No. 51471037) and a Project funded by the Priority Academic Program Development of Jiangsu Higher Education Institutions are greatly acknowledged.

References

- [1] M.R. Joyce, C.M. Styles, P.A.S. Reed, *Int. J. Fatigue* 25 (2003) 863–869.
- [2] C.Y. Jeong, *Mater. Trans.* 53 (2012) 234–239.
- [3] Z. Qian, X.F. Liu, D.G. Zhao, G.Q. Zhang, *Mater. Lett.* 62 (2008) 2146–2149.
- [4] E. Clouet, A. Barbu, L. Lae, G. Martin, *Acta Mater.* 53 (8) (2005) 2313–2325.
- [5] S.K. Shaha, F. Czerwinski, W. Kasprzak, J. Friedmana, D.L. Chena, *J. Alloys Compd.* 615 (2014) 1019–1031.
- [6] W. Kasprzak, B.S. Amirkhiz, M. Niewczas, *J. Alloys Compd.* 595 (2014) 67–79.
- [7] D. Srinivasan, K. Chattopadhyay, *Mater. Sci. Eng. A* 304 (2001) 534–539.
- [8] V.C. Gudla, K. Rechendorff, Z.I. Balogh, T. Kasamac, R. Ambata, *Mater. Des.* 89 (2016) 1071–1078.
- [9] T. Gao, A. Ceguerra, A. Breen, X. Liu, Y. Wu, S. Ringer, *J. Alloys Compd.* 674 (2016) 125–130.
- [10] H. Li, Z. Gao, H. Yin, H. Jiang, X. Su, J. Bin, *Scr. Mater.* 68 (1) (2013) 59–62.
- [11] T. Yoshikawa, K. Morita, *ISIJ Int.* 47 (2007) 582–584.
- [12] T. Yoshikawa, K. Morita, *ISIJ Int.* 45 (2005) 967–971.
- [13] Y. Lei, W. Ma, L. Sun, J. Wu, K. Morita, *Sep. Purif. Technol.* 162 (2016) 20–23.
- [14] Y. Lei, W. Ma, L. Sun, J. Wu, Y. Dai, K. Morita, *Sci. Technol. Adv. Mater.* 17 (1) (2016) 12–19.
- [15] T. Gao, D. Li, Z. Wei, X. Liu, *Mater. Sci. Eng. A* 552 (2012) 523–529.
- [16] O. Schob, H. Nowotny, F. Benesovsky, *Plasenseber. fuer Pulvermetall.* 10 (1962) 65–71.
- [17] A. Raman, K. Schubert, *Z. Met.* 56 (1965) 44–52.
- [18] J.K. Jain, S.P. Gupta, *Mater. Charact.* 49 (2003) 139–148.
- [19] T. Hirano, H. Ohtani, M. Hasebe, *High. Temp. Mater. Process. Lond.* 29 (2010) 347–371.
- [20] P. Dörner, E.-Th Henig, H. Krieg, H.L. Lukas, G. Petzow, *Calphad* 4 (1980) 241–254.
- [21] N. Chakraborti, H.L. Lukas, *Calphad* 16 (1992) 79–86.
- [22] J. Gröbner, H.L. Lukas, F. Aldinger, *Calphad* 20 (1996) 247–254.
- [23] A.T. Dinsdale, *Calphad* 15 (1991) 317–425.
- [24] N. Saunders, V.G. Rivlin, *J. Mater. Sci. Technol.* 2 (1986) 521–527.
- [25] J. Murray, A. Peruzzi, J.P. Abriata, *J. Phase Equilib.* 13 (3) (1992) 277–291.
- [26] H. Okamoto, *J. Phase Equilib.* 23 (5) (2002) 455.
- [27] T. Wang, Z. Jin, J.C. Zhao, *J. Phase Equilib.* 22 (2001) 544–551.
- [28] E. Fischer, C. Colinet, *J. Phase Equilib. Diffus.* 36 (5) (2015) 404–413.
- [29] H.M. Chen, F. Zheng, H.S. Liu, L.B. Liu, Z.P. Jin, *J. Alloys Compd.* 468 (1) (2009) 209–216.
- [30] G. Effenberg, S. Ilyenko, *Materials Science International Services GmbH*, 2005, p. 37. Stuttgart, Germany.
- [31] P. Villars, A. Prince, H. Okamoto, *Asm Intl* 10 (1995).
- [32] M.E. Drits, E.S. Kadaner, V.I. Kuzmina, *Lzv.akad. Nauk. Met.* 1 (1968) 102–105.
- [33] M. Harmelin, K. Girgis, A. Prince, *Ternary alloys* 8 (1993) 354–358.
- [34] S.L. Chen, S. Daniel, F. Zhang, Y.A. Chang, X.Y. Yan, *Calphad* 26 (2) (2002) 175–188.